Corrosion Science 110 (2016) 134–142

Contents lists available at ScienceDirect

Corrosion Science

journal homepage: www.elsevier.com/locate/corsci

Effects of chloride and oxygen on stress corrosion cracking of cold worked 316/316L austenitic stainless steel in high temperature water

Donghai Du [a], Kai Chen [a], Hui Lu [a], Lefu Zhang [a,*], Xiuqiang Shi [b], Xuelian Xu [b], Peter L. Andresen [c]

[a] School of Nuclear Science and Engineering, Shanghai Jiao Tong University, Shanghai 200240, PR China
[b] Shanghai Key Laboratory for Nuclear Power Engineering, Shanghai 200233, PR China
[c] GE Global Research, One Research Circle CE 2513, Schenectady, NY 12309, USA

ARTICLE INFO

Article history:
Received 25 March 2016
Accepted 21 April 2016
Available online 22 April 2016

Keywords:
A. Austenitic stainless steel
C. Stress corrosion cracking
C. High temperature water
C. Cold working

ABSTRACT

Cold work of materials, dissolved oxygen and chloride in water are crucial factors that accelerate the stress corrosion cracking (SCC) crack growth rate of stainless steel in high temperature water. Cold worked austenitic stainless steel type 316 and 316L were studied in order to obtain their effects on SCC crack growth rates in 288 and 325 °C water. Similar SCC behavior were identified for 316 and 316L. Cold working induced comparatively high crack growth rate up to 10^{-8} mm/s even in hydrogenated water, and the collaboration of dissolved oxygen and chloride in water accelerated the SCC crack growth rates much more significantly.

1. Introduction

It has been well recognized that sensitization is the major cause of short stress corrosion crack initiation time and high crack growth rates (CGR) in components made of austenitic stainless steels under normal water chemistry (NWC) in boiling water reactor (BWR) nuclear power plants. The change to low carbon stainless steels, niobium and titanium stabilized stainless steel and hydrogenated water chemistry (HWC) has significantly reduced the occurrence of SCC failures due to sensitization [1–4].

In pressurized water reactor (PWR) nuclear power plant systems, many SCC failures of primary loop components were found to be associated with cold work [5–7] and poor localized water chemistry [8,9]. Ilevbare et al. [9] reported that 53% of the PWR component failures were associated with cold work from a metallurgical point of view, and 83% of all the events related to abnormal chemistry conditions from a water chemistry point of view. Laboratory tests [10–14] also confirmed that cold worked austenitic stainless steels have much higher SCC susceptibility than the solution annealed materials. Many researchers found that impurities in water, such as chloride and sulfate, even at μg/kg (10^{-9}) levels, can accelerate the crack growth rates of sensitized and non-sensitized stainless steels remarkably if the corrosion potential (ECP) was high [15–20].

Degraded insulations and sealing materials, leaked chillers, and decomposed resin fines from demineralizers release detrimental anionic impurities, such as Cl^-, SO_4^{2-} into the coolant water. These anionic impurities are very likely to concentrate in occluded regions, such as crevices, and stagnant dead-leg areas, and reduce the protectiveness of the oxide films, sometimes inducing pitting and initiating micro-cracks, and accelerating the crack growth rate of cracked component materials, especially cold worked, sensitized austenitic stainless steels and nickel base alloys. Abnormal release of impurities trapped in demineralizer resin beds may also happen occasionally, elevating the detrimental impurities level in primary loop, and accelerating the stress corrosion cracking of cold worked stainless steels materials. Furthermore, oxygen can be restained in stagnant ends and occluded regions, such as the omega seals on the control rod driving mechanisms and stagnant pipe ends in auxiliary and safety systems. Thus, presence of dissolved oxygen and anionic impurities at the same regions speeds up the cracking of materials.

In the exception of the SCC events associated with anionic impurities and dissolved oxygen, some SCC incidents were also found in components made of cold worked stainless steels operating under normal hydrogenated PWR water chemistry [10–13,21]. For more than 30 years, nuclear power plant designers had specified that stainless steels be in solution annealed condition for reactor pressure boundary components. Unfortunately, cold work, residual strain, can be introduced from wide variety of processes

* Corresponding author at: Room A332, School of Mechanical Engineering, No. 800 Dongchuan Road, Shanghai 200240, PR China. Fax: +86 21 34205182.
E-mail address: 13524678702@139.com (L. Zhang).

http://dx.doi.org/10.1016/j.corsci.2016.04.035
0010-938X/

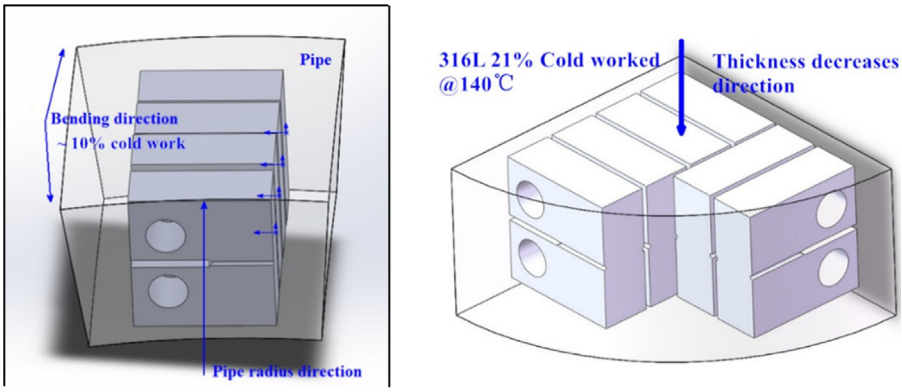

Fig. 1. Specimens from two austenitic stainless steels; a-a PWR primary pipe elbow, type 316 b-21% cold forged block, type 316L.

during component manufacturing, installation and maintenance, for example insufficient annealing heating after forging, cold bending without heat treatment, welding and weld repair, surface cutting or grinding, localized damage due to handling, hydraulic forced aligning, and so on. Welding is commonly used during component installation and repair and it is recognized that 15–25% residual strain can be introduced in the heat affected zone near the fusion lines during welding of austenitic stainless steel.

Although extensive research works have been done previously, there is still lack of reliable data to confirm their distinct effect on SCC crack growth rate. Published data from different laboratories show large variations, sometimes three orders of magnitude, even with the same material and testing conditions. To improve the understanding of SCC mechanisms of cold worked austenitic stainless steels under PWR primary and BWR coolant conditions, and contribute additional experimental data for crack growth rate prediction, the SCC growth rate behavior of cold worked type 316 and 316L 288 and 325 °C to evaluate the effects of chloride and dissolved oxygen and dissolve hydrogen.

2. Testing materials and experimental procedures

2.1. Testing materials

SCC tests were conducted on two pieces of nuclear grade austenitic stainless steels type 316 and 316L. The chemical compositions of these two materials are shown in Table 1. Standard 12.7 mm thickness compact tension (CT) specimens with 5% side grooves on each side were prepared according to Fig. 1. Type 316 specimens were machined in the *R-C* orientation from a cold bended elbow with the maximum deformation of about 10%. Type 316L material was warm pressed at 140 °C to a thickness reduction of 21% and CT specimens were machined in the *S-L* orientation.

Table 1
Chemical compositions of testing materials (wt%).

Elements	C	Si	Mn	P	Cr	Ni	Mo
316	0.046	0.43	1.81	0.012	17.3	12.5	2.48
316L	0.014	0.50	1.80	0.085	17.6	12.4	2.60

Both materials have average grain size of about 100 μm, but the grain size of 316 is much more uniform than 316L.This is because of little grains in 316L produced by higher deformation. No carbide precipitations or secondary phases were observed in either material as shown in Fig. 2. The only major difference between two materials is the content of carbon and deformation level. Moreover, the 316L material for the present work has been studied extensively at GE Global Research and other laboratories world-wide.

2.2. Experimental system

SCC crack growth rates were measured using a facility equipped with an autoclave made of 316L stainless steel, a high precision heating controller, a servo loading system, a direct current potential drop (DCPD) crack length measurement system, and a recirculation water chemistry controlling system which can provide a wide range and precise control of dissolved gases, pH and conductivity. Schematic diagram of the testing facility is given in Fig. 3. A mixed bed demineralizer filled with Rom & Hass DS 160 nuclear grade resin was used to remove anionic and metallic ions from the outlet of an autoclave system. HCl was added into water column that feeds into the autoclave and the injection amount was

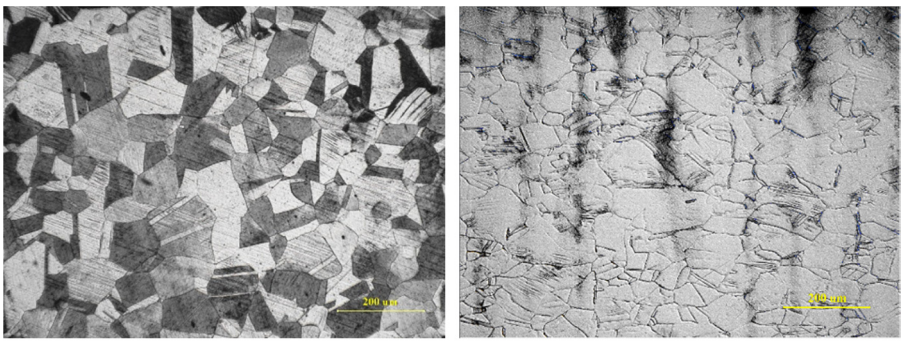

Fig. 2. Metallographic structure of studied material.

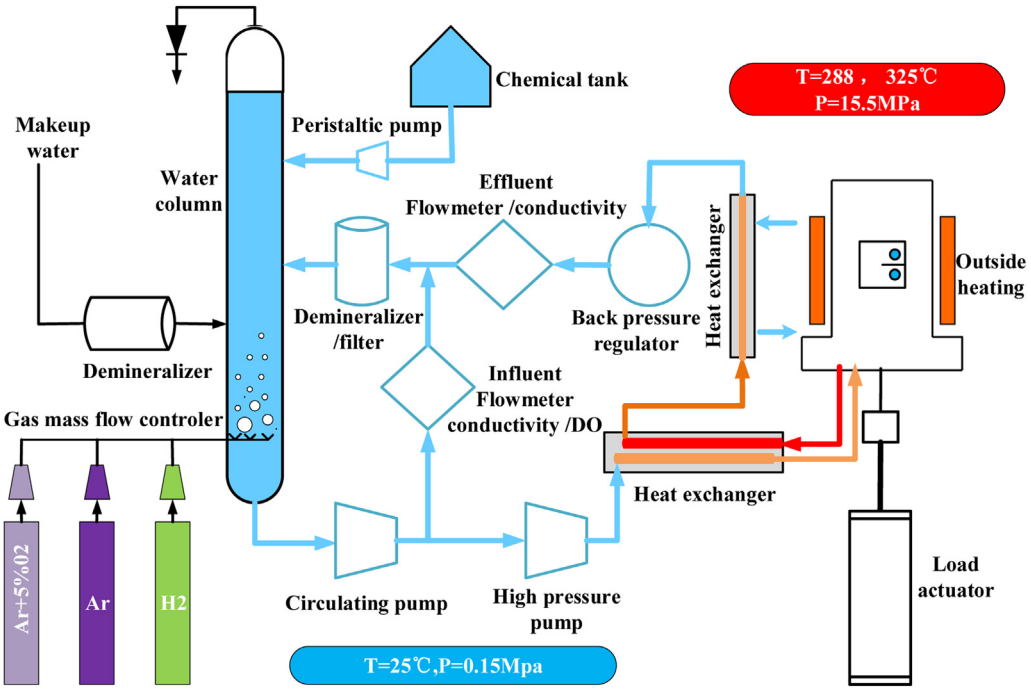

Fig. 3. Schematic diagram of the SCC testing facility.

controlled by inlet conductivity meter. Conductivities of autoclave inlet and outlet water were continuously monitored and recorded by computer.

Dissolved oxygen (DO) in the water was controlled by continuously bubbling high purity argon gas or mixed gases into the water column. About 2000 μg/kg of DO was gotten by bubbling mixed gas of 5% oxygen in high purity argon. Dissolved hydrogen was controlled by bubbling high purity hydrogen regulating of pressure of the water column.

Stable water chemistry in the autoclave was maintained by keeping a stable outlet flow rate above 6 L/h, corresponding to more than 2 autoclave volumes of refresh rate per hour. The operating pressure was regulated by a high precision back pressure regulator and the pressure fluctuation in the autoclave was ±0.2 MPa. The autoclave inlet and outlet conductivities were below 0.06 μS/cm and 0.10 μS/cm respectively at 325 °C during tests in high purity water. The electrochemical corrosion potential was monitored using a Cu/Cu_2O (in ZrO_2 tube) reference electrode and a Pt coupon installed in the autoclave. Water temperature in the autoclave was monitored and controlled using two thermocouples positioned above and below the CT specimen in the autoclave. Less than 1.5 °C difference between two thermocouples was maintained to ensure a homogenous temperature distribution around the CT specimen. A temperature variation of less than ±0.1 °C was attained at steady state by high two precise temperature controllers featuring artificial intelligence (adaptive learning).

SCC crack length was measured by the DCPD system. The current flowing through the CT specimen was reversed about every 0.5 s. The specimen was electrically isolated from loading pins and clevises with zirconia sleeves and spacers. Pt wires were spot welded to the specimen for active and reference potential probes and current leads. Measurement noise was carefully controlled, and the peak-to-peak noise in the DCPD measurement of the testing system typically corresponds to less than 4 μm of crack length during test. The load on CT specimen was actively applied by servo-electric loading system. Different loading modes can be programed to conduct cyclic loading for fatigue pre-cracking, ramp loading and hold at maximum load for transition from pre-crack into SCC crack, and

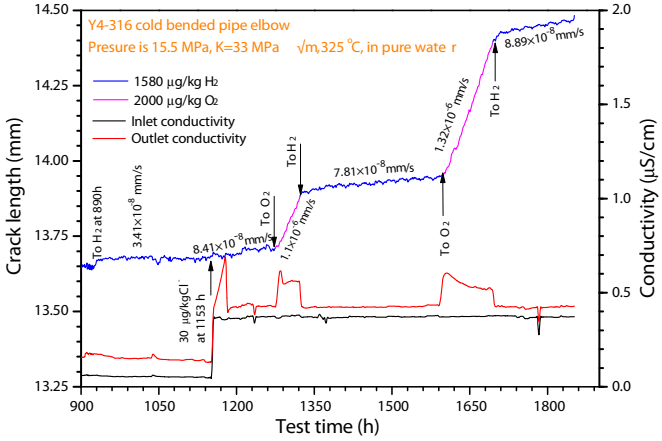

Fig. 4. Crack growth response of specimen Y4 cold bended pipe 316.

constant stress intensity (K) or constant load for SCC crack growth rate measurements. Various waveforms, such as sinusoidal, trapezoid, triangular forms, can be applied for corrosion fatigue tests.

2.3. Experimental procedures

A complete SCC crack growth rate test usually includes three stages, fatigue pre-cracking, transition and SCC crack growth measurements. First fatigue pre-cracking is conducted in high temperature water then a transition from a fatigue crack to a stress corrosion crack is carried out under very low frequency fatigue load, so that the crack morphology and plastic zone size at the crack tip is characteristic of a stress corrosion crack. Finally, SCC crack growth rate measurements are undertaken when the testing condition are stable.

A fatigue pre-crack of about 1 mm in length from the machined notch was produced by increasing load ratio R ($R = K_{min}/K_{max}$) from 0.3 up to 0.5 then to 0.7, at a frequency of above 0.5 Hz, with a K_{max} below the constant K_{max} setting point to be used during SCC tests.

Table 2
Testing sequence and conditions.

Material	Step	T (°C)	DO (μg/kg)	Cl^- (μg/kg)	K (MPa $m^{1/2}$)
316	1	325	<5	0	33
	2		<5	30	
	3		2000	30	
	4		<5	30	
	5		2000	30	
	6		<5	30	
316L	1	325	2000	0	27.5
	2		<5	0	
	3		2000	0	
	4		2000	30	
	5		<5	30	
	6		2000	30	
	7		<5	30	
	8		<5	0	
	9	288	<5	0	27.5
	10		2000	0	
	11		2000	30	
	12		<5	30	
	13		2000	30	
	14		<5	30	

As R is raised, the fatigue crack growth rate slows down, the crack morphology changes to intergranular, and the plastic zone at the crack tip becomes characteristic of SCC.

Subsequent transitioning procedure was performed in high temperature water environment by cycling at R = 0.7 and 0.001 Hz, and after well-behaved crack advance was observed, introducing a hold time of 9000 s at K_{max}. After the crack grew for a length of more than one or two grain size, a change to constant K was made and a stable SCC growth rate was evaluated over at least one grain size.

Testing conditions during normal stage of SCC crack growth rate measurement are listed in Table 2. It is very important to get the crack growth rates of each material in oxygenated water before studying the effect of chloride. The SCC crack growth rates in oxygenated water was considered as a baseline data for evaluating SCC growth rates under other conditions. Reproducibility was checked to confirm that the operation of testing system was stable and SCC cracking was well behaved. This can be achieved by changing water chemistry between oxygenated to hydrogenated water, or adding and removing impurities, and is often repeated at two times. The reproducibility is confirmed if the crack growth rates in same testing condition are very close.

After the SCC test, specimens were electro-discharge machined into two halves in the thickness direction. One half of specimen was further sliced into 4 or 5 pieces for cross-sectional observation of the cracking morphology, microstructure characterization, crack length measurement etc. The other half was fractured by fatigue in air, exposing the crack surface for further observation. Optical microscopy, scanning electron microscopy (SEM) and electron back scattered diffraction (EBSD) were used to examine the fracture surfaces and SCC crack morphology. Good agreement was observed between the DCPD crack length measurement results and post-test crack length observation.

3. Results

3.1. SCC crack growth rate

The crack growth profile of specimen Y4 cold bended pipe 316 is shown in Fig. 4. The data of the initial 900 h is not presented here due to its irrelevance to the current study. The crack growth rate in 2000 μg/kg oxygenated high purity water is about 6.7×10^{-7} mm/s, consistent with our previous result [22]. The crack growth rate

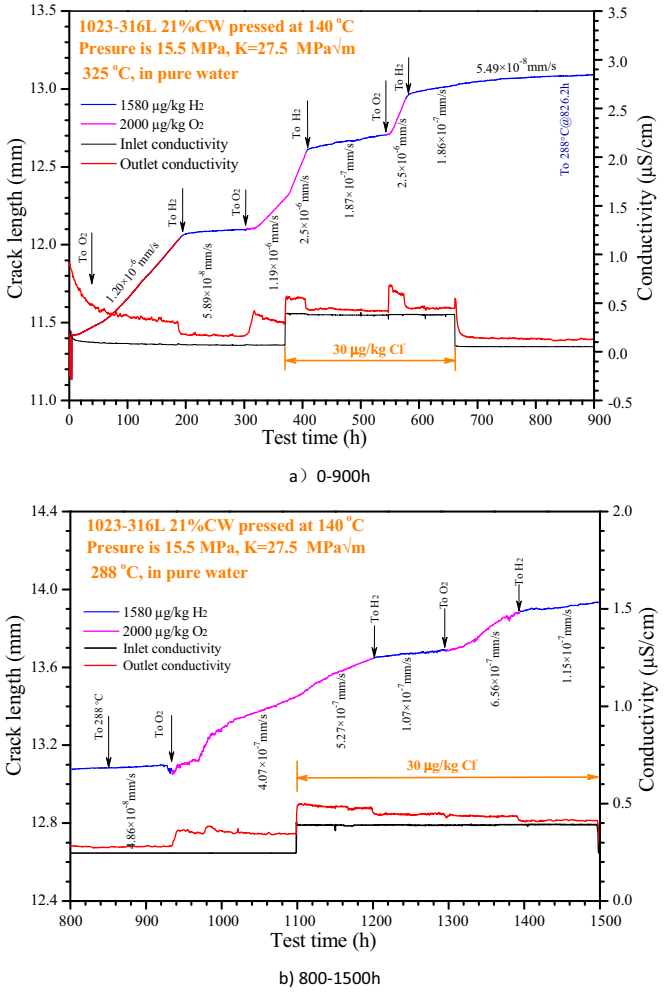

Fig. 5. SCC growth rate response of specimen 1023 warm cold worked 316L.

in HWC condition was 3.41×10^{-8} mm/s. After adding 30 μg/kg Cl^- the crack growth rate started to increase (from 1153 h to test end in Fig. 4) and a stable crack growth rate of 8.41×10^{-8} mm/s was obtained in HWC. The addition of 2000 μg/kg oxygen at 1283 h produced a significant increase in crack growth rate of 1.1×10^{-6} mm/s. On returning back to HWC condition, the CGR decreased and stabilized at 7.81×10^{-8} mm/s, which is quite close to the prior value of 8.41×10^{-8} mm/s obtained before under the same conditions. Changing back to 2000 μg/kg oxygen at 1600 h, crack growth rate increased again to 1.32×10^{-6} mm/s. The crack growth rate of 8.89×10^{-8} mm/s was gotten in HWC condition at the end of the test. Good reproducibility can be found under the same water chemistry condition and this is what we called the reliability of data. Obviously, Cl^- accelerates the SCC CGR of 316 in water, and the CGRs under HWC conditions are much lower than that in oxygenated water.

Fig. 5(a) shows the crack growth response of the 316L specimen during testing at 325 °C. The SCC response of 316L was similar to 316 under the corresponding water chemistry conditions. The crack growth rates of 316L under reducing (1580 μg/kg H_2) and oxidizing (2000 μg/kg DO) conditions were 5.89×10^{-8} mm/s and 1.2×10^{-6} mm/s, respectively. When 30 μg/kg Cl^- was added at 373 h, the SCC crack growth rate increased immediately and finally achieved a steady growth rate of 2.5×10^{-6} mm/s. The crack growth rate dropped to 1.87×10^{-7} mm/s on changing to HWC at ~407 h. The addition of Cl^- was stopped at 660 h and the residual Cl^- in the water was removed by demineralizer over ~2 h. The SCC crack

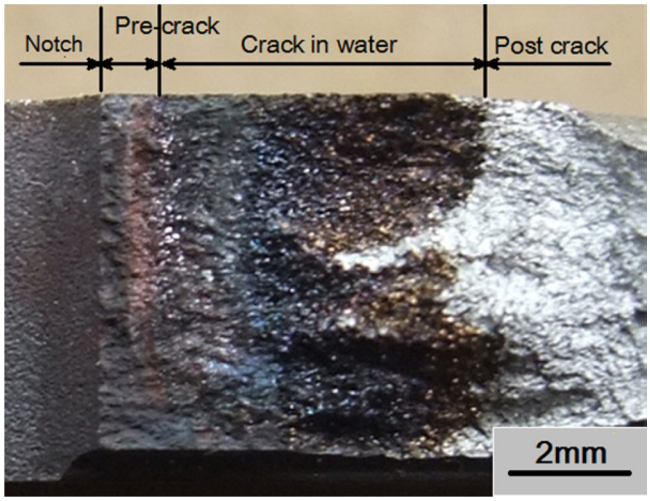

Fig. 6. Optical morphology of the fracture surface of the specimen Y4 cold bended pipe 316.

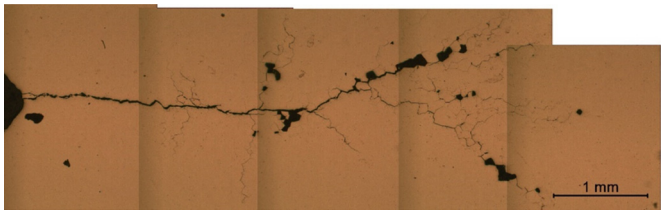

Fig. 7. Morphology of the SCC propagation path of the specimen Y4 cold bended pipe 316.

growth rate decreased to 5.49×10^{-8} mm/s until 825 h. The high repeatability of the SCC crack growth rates under HWC conditions before the addition and after the removal of Cl^- also proves that SCC crack growth rate is not affected by the prior testing condition.

To study the effects of Cl^- on SCC behavior at different temperatures, crack growth rate measurements at the same water chemistry conditions were repeated at temperature of 288 °C. The crack growth rate at 288 °C was established and stabilized at 2.56×10^{-8} mm/s under HWC conditions which is about 2 times lower than at 325 °C. The crack growth rate became negative at 925 h when the bubbling gas changed from hydrogen to a mixed gas of 5% oxygen in argon. This phenomenon may relate to the contact between the fracture surface walls of the crack. To reactivate the crack, trapezoidal wave load was introduced between 925 and 1013 h with $R = 0.7$, f = 0.001 Hz and hold time = 9000 s at K_{max}. After changing to constant K at 1013 h, the crack growth rate increased slowly to 4.07×10^{-7} mm/s. At 288 °C, the acceleration effect of Cl^- decreased 1.3 times and the crack growth rate declined to 1.07×10^{-7} mm/s, when 2000 μg/kg of DO was bubbled in water. The repeat test yielded a slightly higher crack growth rate, which may be related to the slight increase of the real K at the zigzag crack tip comparing with the nominal value of K. The nominal K used for load control is an average of the zigzagged crack front based on DCPD data, and the value may be less than the actual K at the crack front.

3.2. Microstructure observations

Optical microscopy observations of the fracture surfaces of the 316 and 316L specimens are presented in Figs. 6 and 9. The specimen notch, pre-cracking zone, SCC cracking zone in high temperature water and the post air fatigue cracking zone can be easily distinguished. The fracture surfaces of the specimen Y4 cold bended pipe 316 are mostly intergranular. The crack front is not straight and un-cracked regions can be found in the SCC zone. By comparison, the fracture surfaces of the 316L specimen are smoother and the crack front is straighter than the 316. The existence of un-cracked segments on SCC zone of 316 means that SCC susceptibility at different positions was not uniform due to inhomogeneities in the metallurgical microstructure or plastic deformation. Cross section of the SCC cracks from the 316 and 316L specimens are shown in Figs. 7 and 10. The heavily branched cracks and significant secondary cracking in the 316 may result from inhomogeneous deformation. This is because the 316L was deformed in a way that the plastic deformation is much more homogeneous within the specimen and the SCC cracks propagate in a straighter path and exhibit smaller secondary cracks.

Figs. 8 and 11 show the stress corrosion cracking fracture surfaces of cold worked austenitic stainless steel in high temperature water. The morphology of the SCC zone in the 316 is nearly 100% intergranular cracking while the 316L specimen shows predominantly intergranular cracking accompanied by some transgranular cracking (Fig. 11). The EBSD results on the crack tip of the 316L specimen is shown in Fig. 12(c). The cracks on 316L specimen are not strictly along the grain boundary; the crack propagates transgranularly through some grains. Intergranular cracking was found to occur preferentially along random (high energy) grain boundaries; cracking along coincidence site lattice (CSL) boundaries was not found, consistent with previous studies [23].

4. Discussion

The SCC crack growth rates of cold worked 316 and 316L under various water chemistry conditions are summarized in Fig. 13. Both 316 and 316L specimens yield the lowest crack growth

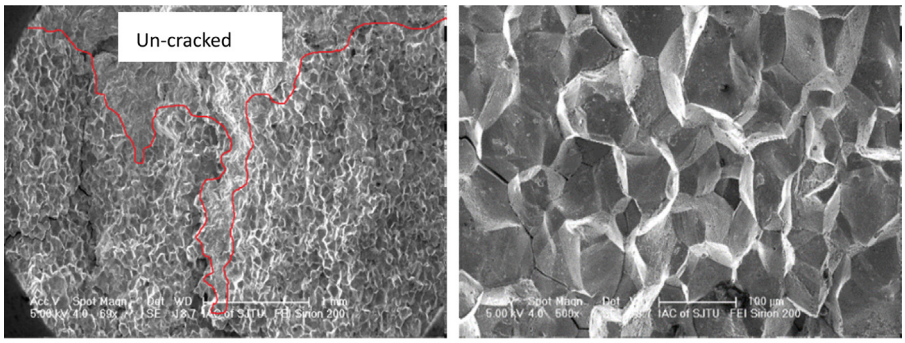

(a) un-cracked part in SCC region (b) typical intergranular cracking

Fig. 8. Typical morphologies of the fracture surface at SCC region on the specimen Y4 cold bended pipe 316.

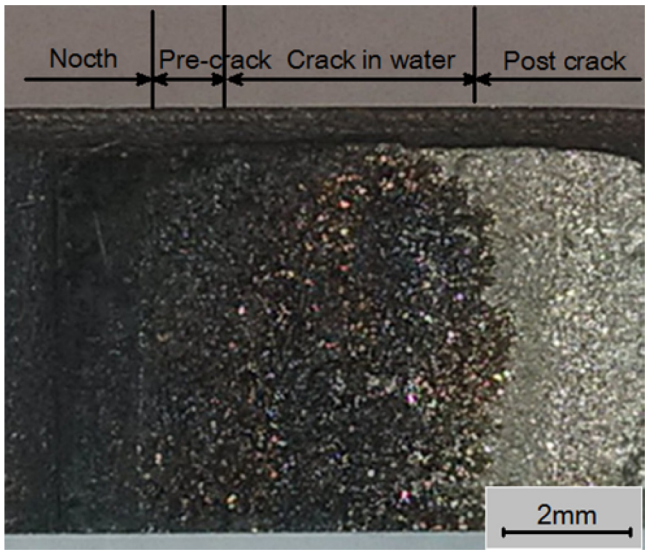

Fig. 9. Fracture surface of warm cold worked nuclear grade 316L stainless steel (specimen 1023).

rates in hydrogenated pure water. Chloride has smaller effect in accelerating their crack growth rates in hydrogenated water compared to DO. Because addition of 30 μg/kg of Cl^- in hydrogenated water only produced a CGR about 3× higher in hydrogenated pure water. The effect of Cl^- was magnified by DO. Dissolved oxygen in water significantly accelerates SCC crack growth rates in these two materials independent of whether the water is pure or contaminated with chloride ion. Stress corrosion cracking CGRs of both materials increased about 20× after changing from hydrogenated to oxygenated pure water at 325 °C, while, in water containing 30 μg/kg of Cl^-, the increase of SCC CGRs is about 15× after changing from hydrogenated to oxygenated water chemistry. Actually, the synergistic effects of Cl^- and dissolved oxygen that accelerates significantly the SCC crack growth rate in high temperature water. Because the crack growth rate of 316/316L increase about 40 times comparing to the CGR value in HWC pure water.

According to the slip-dissolution-oxidation model [2,3], the crack advance per cycle results from disruption of the passive film by shear strain, and accelerated oxidation in that region. At the crack tip, localized mechanical strain (or creep strain) can leads to the exposure of bare metal to corrosive environment at the crack tip, but may also simply damage the inner, protective layer of the oxide, depending on the oxide thickness and slip offset. Oxidation of metal (with very limited dissolution because of the low solubility of metal cations) will occur as a consequence of the damage to the passive film. The rupture and re-passivation time of the passive film and the oxidation rate of metal at crack tip determine the crack growth rate of the material. However, the fracture and re-passivation of the passive film at crack tip are affected by many factors, such as crack tip load (or strain), properties of the film, temperature, crack tip material chemistry and crack tip chemistry.

Andresen and Young [24] show that a low ECP environment in the crack interior develops even in oxygenated water due to the constrained geometry of a SCC crack whose opening is usually of the order of micrometers, coupled with oxygen consumption that is much faster than its diffusion into the crack. Therefore, a corrosion potential gradient at the crack mouth is established as shown in Fig. 14, which is determined by both the external and internal potential of the crack. In hydrogenated water, the external surface sustains a low ECP, and the full length of crack has an internal ECP almost identical to the surface because of no H_2 is consumed in the crack. The crack tip can be at very slightly lower potential because of the release of hydrogen due to corrosion near the crack tip.

According to the crack tip water chemistry model by Andresen, the electrochemical reaction in the crack can be divided mainly into two uncoupled parts, namely macro cell and micro cell which are described in Fig. 14 [24]. The anodic reaction process can be described by [25]:

$$3Fe + 4H_2O \rightarrow Fe_3O_4 + 8H^+ + 8e^- \quad (1)$$

$$Ni + H_2O \rightarrow NiO + 2H^+ + 2e^- \quad (2)$$

$$2Cr + 3H_2O \rightarrow Cr_2O_3 + 6H^+ + 6e^- \quad (3)$$

The bare metal exposed by broken passive film at the crack tip reacts very rapidly with high temperature water and only a low concentration of metal Fe, Ni and Cr dissolve into the water because of

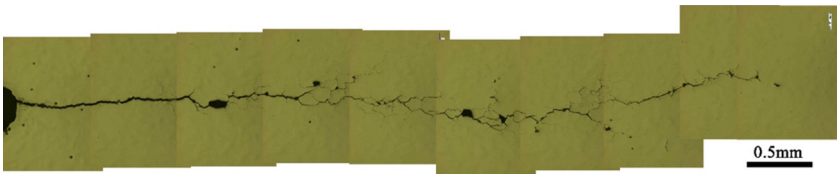

Fig. 10. Cross sectional morphology of crack propagation path in cold worked nuclear grade 316L stainless steel (specimen 1023).

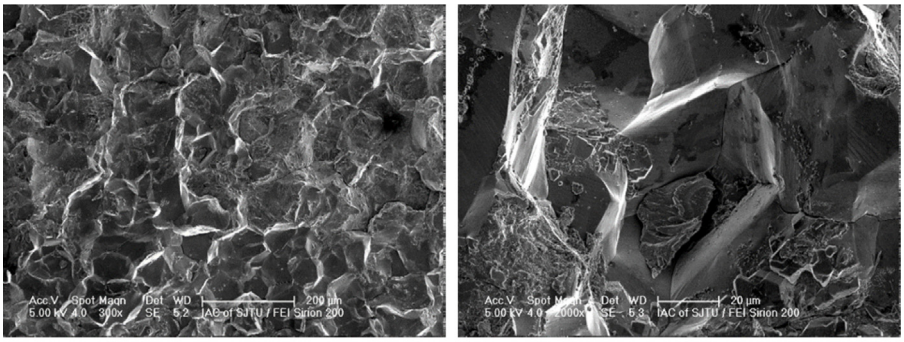

(a) predominant intergranular cracking (b) partially transgranular cracking

Fig. 11. SEM micrographs of SCC region on the fracture surface of 316L (specimen 1023).

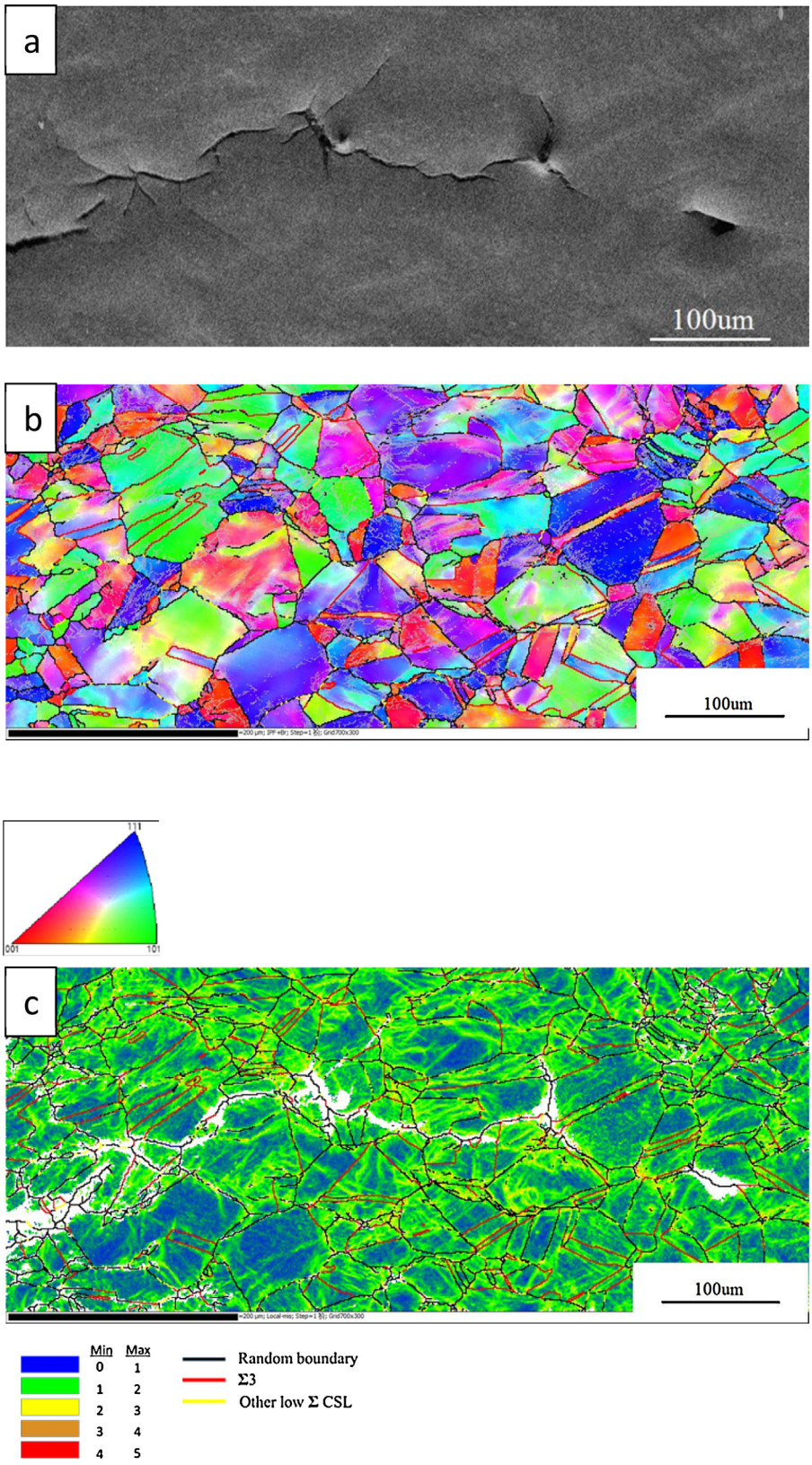

Fig. 12. EBSD results of the crack tip region of the cold worked 316L CT specimen. (a) Morphology of crack path. (b) Inverse pole figure and (c) kernel average mis-orientations and types of the grain boundaries.

their low solubility (except in an aggressive crack tip chemistries). The water in the crack (crevice) is quickly saturated with these metallic cations due to the low cation solubility. With the metallic ions to balance the high concentration of OH^-, the pH in the crack shifts to alkaline direction when exposed to very high purity water containing oxidants. Andresen [15] points out that the change in the solubility of iron, nickel and chromium oxides is 100–1000 fold per unit change in pH in either direction. Metallic cations saturate

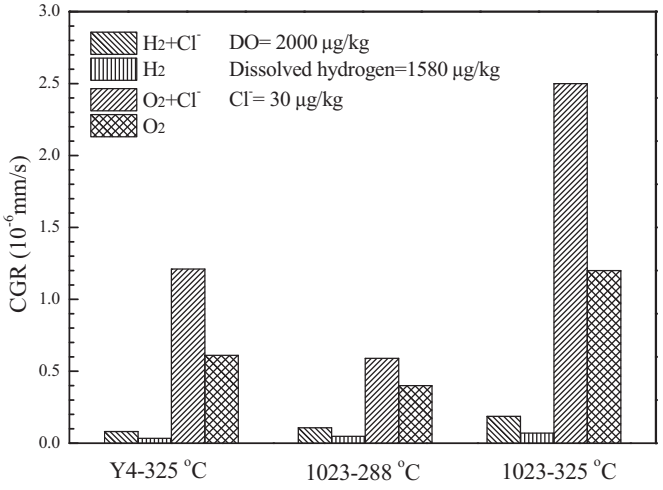

Fig. 13. CGRs of 316 (Y4) and 316L (1023) in various water chemistry conditions.

at the crack tip quickly, and the excess metallic cations either diffuse out of the crack under the force of potential and concentration gradient, or precipitate to form oxide along the crack surfaces. Thus, the SCC crack growth rate increased when oxidants are present in water. The increase in pH at the crack tip is controlled by species such as $HNiO_2^-$ and $HFeO_2^-$ [26].

When impurities such as Cl^- are present, the crack tip becomes acidic because Cl^- is concentrated in the crack and is charge balanced by H^+. Acidification is limited by the back-diffusion of Cl^- out of the crack—at relevant levels of impurities (e.g., ≤30 μg/kg), the concentration of Cl^- at the crack tip is generally limited to ~30–50×.

In hydrogenated water, no potential gradient will be established between crack tip and crack mouth. Hydrogen diffuses into crack and maintains roughly the same fugacity inside as outside the crack, and thus the corrosion potential is essentially identical. With no potential gradient, the opportunity for acidification of alkalization is effectively limited to what occurs in the bulk water. This is the primary reason for low crack growth rate in stainless steel in hydrogenated water chemistry.

From the E-pH diagram [27] shown in Fig. 15, it is easy to understand why passive film in the crack can be damaged easily and metal dissolution rate increases by decreasing the passivation efficiency. When anion impurities are introduced into oxygenated water, the

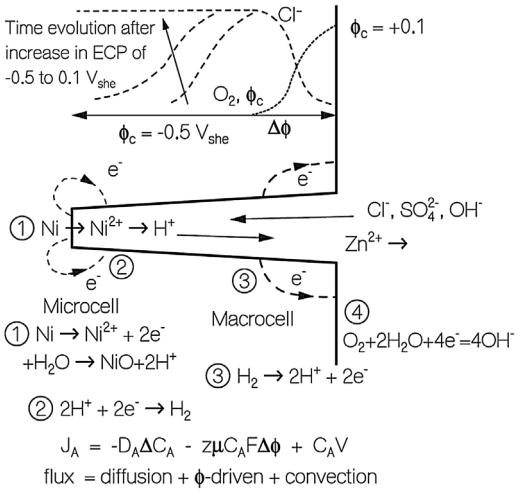

Fig. 14. Schematic of crack tip chemistry forming process [24].

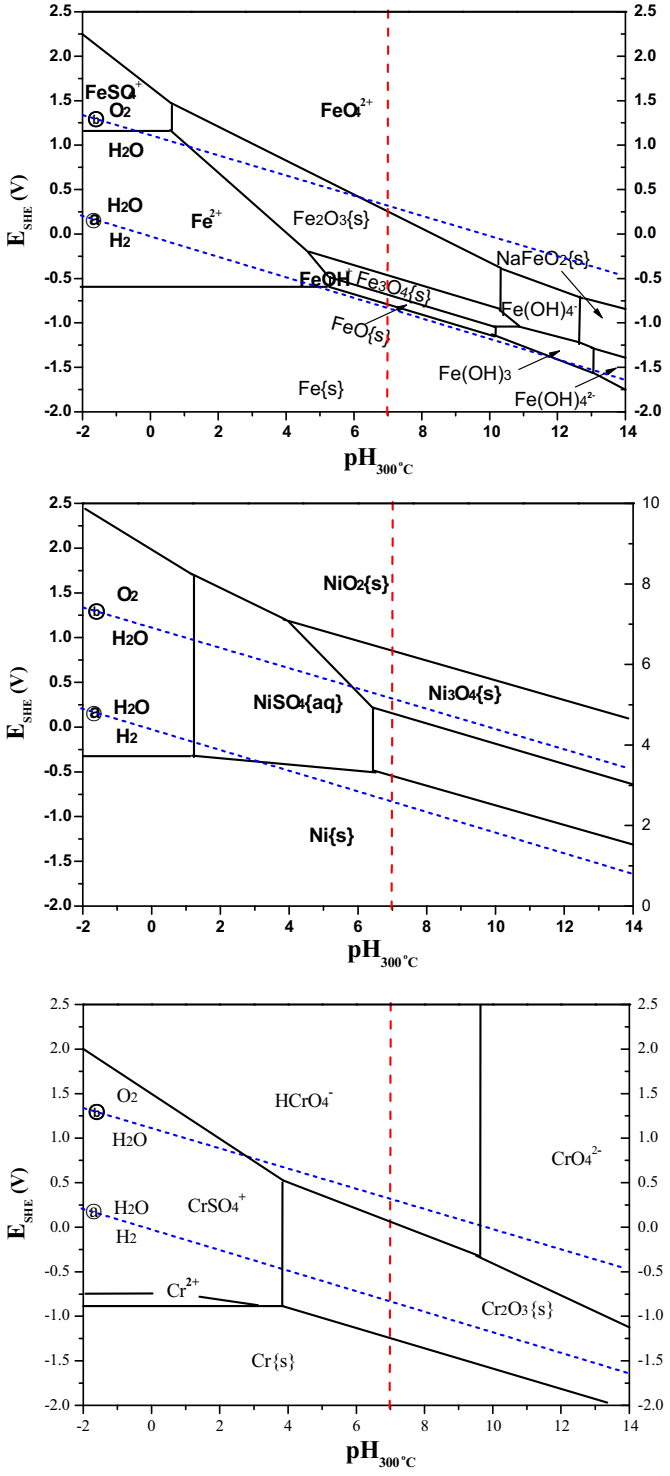

Fig. 15. Potential-pH diagrams for Fe, Ni, Cr calculated at 300 °C and for 10^{-6} M solubility of the soluble species reproduced from Staehle and Gorman [27].

anions will migrate into the crack under the action of the potential gradient, and will concentrate at the crack tip. If the impurities are species like Cl^- and SO_4^{2-}, acidification occurs at the crack tip (if the impurities only contain OH^- (such as NaOH) then the crack pH can only rise). And this process produces higher corrosion potential in the deaerated crack because of the effect of pH on line @ in Fig. 15, which reduces the potential gradient. Andresen has commented that under relevant BWR conditions, a negative pH shift of 2 might be expected [24]. In addition, the incorporation of Cl^- into crack tip

may reduce the protectiveness of newly formed film by producing higher content of ionic defects or changing the properties of the film.

In hydrogenated water, there exists no consequential potential gradient in the crack and crack chemistry is basically same as the bulk water. When 30 μg/kg of Cl^- is added, the pH in the bulk water ($pH_{325\,^\circ C}$ = 5.73) changes a little relative to high purity water ($pH_{325\,^\circ C}$ = 5.86). The increased CGRs of 316 and 316L in hydrogenated water may be primarily due to the destructive effect of Cl^- on the composition and properties of the passive film at crack tip.

5. Conclusions

From above SCC tests carried out to evaluate the effects of Cl^- and DO on the CGR of 316 and 316L stainless steel. The following conclusions can be drawn from the results:

(1) Both DO and Cl^- can accelerate CGRs of cold worked 316 and 316L to some extent, but the major factor is DO.
(2) The reason DO and chloride significantly accelerate SCC crack growth rate is the change of pH in the crack and the destruction of crack tip passive film by Cl^-.
(3) The deformation level and homogeneity affect the morphology of SCC fracture surface. Transgranular cracking prone to occur on higher level cold worked 316 and 316L stainless steel.

Acknowledgements

Thanks to Roger W. Staehle for his help in analyzing thermodynamics and electrochemistry in high temperature water. Thanks to Liu Tingguang of Shanghai University for his help in the EBSD analysis. This work is financial supported by the National Science and Technology Major Project of the Ministry of Science and Technology of China, under project No. 2011ZX06004-009-0601.

References

[1] F.P. Ford, P.L. Andresen, Fundamental modeling of environmental cracking for improved design and lifetime evaluation in BWRs, Int. J. Presv. Vessels Pip. 59 (1994) 61–70.
[2] P.L. Andresen, F.P. Ford, Life prediction by mechanistic modelling and system monitoring of environmental cracking of Fe and Ni alloys in aqueous systems, Mater. Sci. Eng. A 103 (1988) 167–183.
[3] P.L. Andresen, Perspective and direction of stress corrosion cracking in hot water, in: Proc. of Tenth Int. Symp. on Env. Degradation of Materials in Nuclear Power Systems—Water Reactors, Houston, TX: NACE, 2001.
[4] S.M. Bruemmer, G.S. Was, Microstructural and microchemical mechanisms controlling intergranular stress corrosion cracking in light-water-reactor systems, J. Nucl. Mater. 216 (1994) 348–363.
[5] N. Matsubara, T. Kobayashi, K. Fujimoto, Y. Nomura, N. Chigusa, S. Hirano, Research program on SCC of cold-worked stainless steel in Janpanese PWR N.P.P. INIS 42 (2011) RN:42088753.
[6] T. Shoji, K. Sakaguchi, Z.P. Lu, S. Hirano, Y. Hasegawa, T. Kobayashi, K. Fujimoto, Y. Nomura, Effects of Cold Work and Stress on Oxidation and SCC Behavior of Stainless Steels in PWR Primary Water Environments, INIS, 2011, pp. 50–62.
[7] Z.P. Lu, T. Shoji, Y. Takeda, Y. Ito, A. Kai, S. Yamazaki, Transient and steady state crack growth kinetics for stress corrosion cracking of a cold worked 316L stainless steel in oxygenated pure water at different temperatures, Corros. Sci. 50 (2008) 561–575.
[8] R. Kilian, R. Zimmer, G. Maussner, G. König, Intergranular stress corrosion cracking of SS in LWRs, in: EPRI/AECL Workshop on Cold Work and Its Impact on Components in Light Water Nuclear Reactors, Toronto, Canada, June 4–8, 2007.
[9] G.O. Ilevbare, F. Cattant, N.K. Peat, SCC of Stainless Steels under PWR Service Conditions, 42, INIS, 2011, RN:42088756.
[10] K. Arioka, T. Yamada, T. Terachi, R.W. Staehle, Intergranular stress corrosion cracking behavior of austenitic stainless steels in hydrogenated high-temperature water, Corrosion 62 (2006) 74–83.
[11] P.L. Andresen, M.M. Morra, IGSCC of non-sensitized stainless steels in high temperature water, J. Nucl. Mater. 383 (2008) 97–111.
[12] Q.J. Peng, J. Hou, T. Yonezawa, T. Shoji, Z.M. Zhang, F. Huang, E.-H. Han, W. Ke, Environmentally assisted crack growth in one-dimensionally cold worked Alloy 690TT in primary water, Corros. Sci. 57 (2012) 81–88.
[13] T. Terachi, T. Yamada, T. Miyamoto, SCC growth behaviors of austenitic stainless steels in simulated PWR primary water, J. Nucl. Mater. 426 (2012) 59–70.
[14] F.J. Meng, Z.P. Lu, T. Shoji, Stress corrosion cracking of uni-directionally cold worked 316NG stainless steel in simulated PWR primary water with various dissolved hydrogen concentrations, Corros. Sci. 53 (2011) 2558–2565.
[15] P.L. Andresen, Effects of transients in water chemistry temperature and loading on intergranular stress corrosion cracking of AISI 304 stainless steel, Corrosion 42 (1986) 169–180.
[16] P.L. Andresen, Effects of specific anionic impurities on environmental cracking of austenitic materials in 288 °C water, Proc. of Fifth International Symposium on Environmental Degradation of Materials in Nuclear Power Systems—Water Reactors, ANS (1992) 209–218.
[17] B. Gordon, S. Garcia, Effect of Water Purity on Intergranular Stress Corrosion Cracking of Stainless Steel and Nickel Alloys in BWRs, 42, INIS, 2011, RN:42088761.
[18] J. Congleton, H.C. Shih, T. Shoji, R.N. Parkins, The stress corrosion cracking of type 316 stainless steel in oxygenated and chlorinated high temperature water, Corros. Sci. 25 (1985) 769–788.
[19] L. Ljungberg, D. Cubicciotti, M. Trolle, Effects of impurities on the IGSCC of stainless steel in high-temperature water, Corrosion 44 (1988) 66–72.
[20] H.P. Hermansson, K. Gott, I. Vatter, A. Crossley, G. Cattle, Mechanism for the effect of sulphate on SCC in BWRs, in: Swedish Nuclear Power Inspectorate, SKI, Stockholm, 1997, SKI Report 97:35.
[21] P.L. Andresen, P.W. Emigh, M.M. Morra, J. Hickling, Effects of PWR primary water chemistry and deaerated water on SCC, in: Proc. 12th Int. Symp. on Environmental Degradation of Materials in Nuclear Power System—Water Reactors, TMS, Snowbird, August, 2005.
[22] D.H. Du, K. Chen, L. Yu, H. Lu, L.F. Zhang, X.Q. Shi, X.L. Xu, SCC crack growth rate of cold worked 316L stainless steel in PWR environment, J. Nucl. Mater. 456 (2015) 228–234.
[23] Z.P. Lu, T. Shoji, F.J. Meng, H. Xue, Y.B. Qiu, Y. Takeda, K. Negishi, Characterization of microstructure and local deformation in 316NG weld heat-affected zone and stress corrosion cracking in high temperature water, Corros. Sci. 53 (2011) 1916–1932.
[24] P.L. Andresen, L.M. Young, Characterization of the roles of electrochemistry, convection and crack chemistry in stress corrosion cracking, Proc. 7th Int. Symp. on Environmental Degradation of Materials in Nuclear Power Systems—Water Reactors, NACE (1995) 579–596.
[25] A. Turnbull, Modelling of crack chemistry in sensitized stainless steel in boiling water reactor environments, Corros. Sci. 39 (1997) 789–805.
[26] D.F. Taylor, Crevice corrosion of Alloy 600 in high temperature aqueous environments, Corrosion 35 (1979) 550–559.
[27] R.W. Staehle, J.A. Gorman, Quantitative assessment of submodes of stress corrosion cracking on the secondary side of steam generator tubing in pressurized water reactors: part 1, Corrosion 59 (2003) 931–994.